SCIENCE AND TECHNOLOGY OF ADVANCED MATERIALS
2025, VOL. 26, NO. 1, 2515007
https://doi.org/10.1080/14686996.2025.2515007

Taylor & Francis
Taylor & Francis Group

Merging π-molecular functions achieved through homogeneous liquid-liquid blending of solvent-free alkyl-π liquids

Zhenfeng Guo [a,b,c], Chengjun Pan [b], Akira Shinohara [c] and Takashi Nakanishi [a,c]

[a]Division of Soft Matter, Graduate School of Life Science, Hokkaido University, Sapporo, Japan;
[b]College of Materials Science and Engineering, Shenzhen University, Shenzhen, China;
[c]Research Center for Materials Nanoarchitectonics (MANA), National Institute for Materials Science (NIMS), Tsukuba, Japan

ABSTRACT

Solvent-free alkyl-π liquids, an emerging class of optoelectronically-active soft materials, have attracted attention for their applications in soft electronics, offering liquid fluidity as well as predictable and stable π-functions. Extensive research has been conducted to date on controlling the optoelectronic properties of alkyl-π liquids. When modulating function by adding solid dopants, the dopant molecules have poor solubility, leading to insoluble aggregates and inconsistencies in properties such as luminescent color. Chemical modification of the π-skeleton requires synthesizing molecules that display the desired properties, which poses challenges in achieving predictable performance and ensuring economic feasibility across various molecular designs. In this study, we propose a liquid-liquid blending strategy that enables the precise and homogeneous merge of π-functions of alkyl π-liquids. Rheological analysis was used to evaluate miscibility between alkyl π-liquids. Furthermore, the accurate and uniform control of the photoluminescent color––a representative π-function––was successfully demonstrated through the blending of three alkyl π-liquids that emit the three primary colors. This liquid-liquid blending strategy offers an innovative approach for adjusting not only luminescent color but also for merging various π-functions in solvent-free liquid materials.

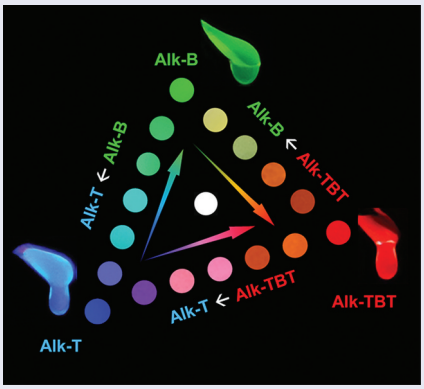

IMPACT STATEMENT

Merging of π-function was established through homogeneous blending of alkyl-π liquids and verified by rheology, which allows for accurate control of photoluminescent color in binary and ternary liquid blends.

ARTICLE HISTORY
Received 1 May 2025
Revised 27 May 2025
Accepted 29 May 2025

KEYWORDS
Alkyl-π liquids; miscibility; homogeneous blends; rheology; luminescent color tuning

1. Introduction

Merging distinct functions within a singular class of materials presents a considerable challenge, chiefly attributable to the phase separation tendencies prevalent in heterogeneous systems, such as metal alloys [1,2] and polymer blends [3,4]. Upon the occurrence of phase separation, the material's function becomes non-uniform, leading to a composite of distinct functions rather than a singular, unified one [5–7]. This results in, for instance, mechanical properties that are intricate and challenging to anticipate [8]. In developing organic molecular materials, comprehensive research has emphasized the effective use of self-assembly [9–16], supramolecular complexation [17–

CONTACT Chengjun Pan pancj@szu.edu.cn College of Materials Science and Engineering, Shenzhen University, Shenzhen, China; Takashi Nakanishi nakanishi.takashi@nims.go.jp Research Center for Materials Nanoarchitectonics (MANA), National Institute for Materials Science (NIMS), 1-1 Namiki, Tsukuba 305-0044, Japan

Supplemental data for this article can be accessed online at https://doi.org/10.1080/14686996.2025.2515007

20], and controlled phase separation [21–24], achieved through proficient manipulation of intermolecular interactions. Nevertheless, when the objective is to guarantee consistent material properties and accommodate intricate deformations for soft electronics applications, a comprehensive molecular design is imperative. This design ought to reflect the inherent functions of the active units with minimal alteration while preserving significant deformability. One promising approach to realizing these design principles involves utilizing alkyl-π functional molecular liquids (alkyl-π liquids) [25–37].

In alkyl-π liquids, the bulky yet flexible branched alkyl chains encase and protect the optically and electronically active π-conjugated core, thereby augmenting its photostability [34,38]. In recent years, there has been a surge in research on functional π-liquid materials that exhibit luminescent [28,32,33,39,40], electrochromic [41,42], mechanochromic [43,44], thermoresponsive [39,43–47], and electret properties [34,48–50], among other features derived from π-conjugated systems [27,30,31,51,52]. In alkyl-π liquids, it is often necessary to fine-tune the π-functions to meet specific application requirements. Two major strategies have been reported thus far. The first is functional modulation through doping, which involves incorporating dopant molecules into alkyl π-liquids [39,53,54]. This technique primarily modifies luminescent color, enabling multi-color luminescence [39,55,56] or even white luminescence [54,57]. Nevertheless, the limited solubility of solid dopants frequently leads to aggregation, thereby compromising the uniformity of their properties and restricting the advancement of materials more broadly [58,59]. The second approach involves chemically modifying the π-conjugated core to produce unique liquid molecules with customized optical properties [59–61]. Although this method can ensure uniform luminescence in a single color, it necessitates the meticulous design and synthesis of individual, distinct molecules, which poses challenges in achieving predictable performance and maintaining economic viability across various molecular designs.

In this study, we propose a liquid-liquid blending strategy aimed at achieving precise control over the π-function of alkyl π-liquids. We initially illustrate that time-temperature superposition (TTS) in rheological analysis assesses the miscibility of alkyl π-liquids possessing analogous physical characteristics. Subsequently, by employing photoluminescence––a representative π-function––as a probe, we synthesize three solvent-free alkyl-π room-temperature liquids that emit red, green, and blue light, respectively. Through blending these liquids in various combinations, we attain uniform and tunable control over the photoluminescent color. This liquid-liquid blending strategy provides an innovative materials design platform for merging diverse π-molecular functions of solvent-free alkyl-π liquids.

2. Results and discussions

2.1. Molecular design and characterization of liquids

We newly designed and synthesized a series of alkyl-π liquids (Alk-TBT, Alk-B, and Alk-T, in Figure 1a). Based on the 'alkyl-π engineering' strategy [38] (controlling the state of alkyl-π molecules by taking a balance between the van der Waals forces of the alkyl chains and π-π interactions), three alkylated *bis*-phenylene derivatives were designed. While introducing 2-octyldodecyl Guerbet-type branched alkyl

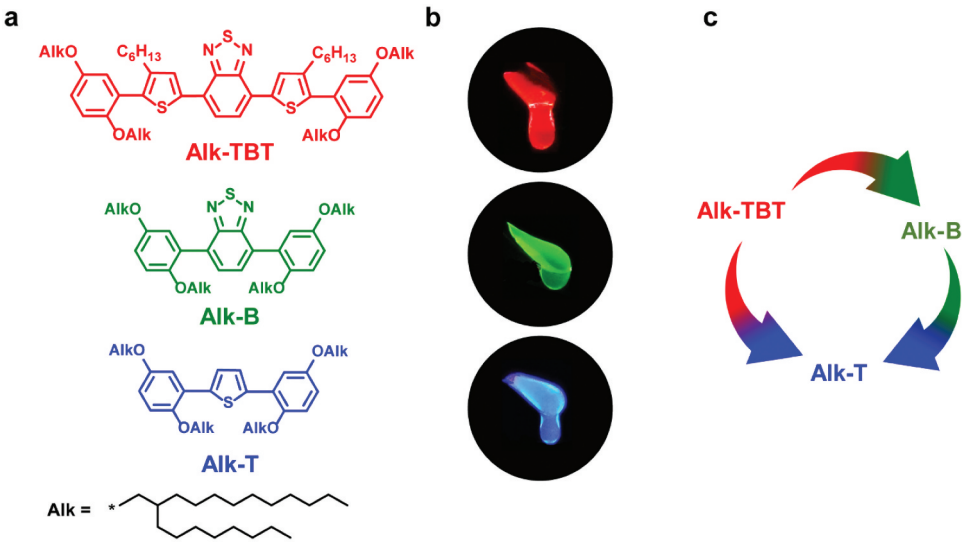

Figure 1. a) chemical structures and b) photographs of Alk-TBT, Alk-B, and Alk-T (from top to bottom) in the liquid state at 23.0 ± 0.5 °C under 365 nm UV light irradiation. c) color tuning schematic diagram. The arrows indicate where the electron acceptor-type liquid is blended with the electron donor-type liquid.

side chains (Alk), benzothiadiazoledithiophene (TBT), benzothiadiazole (B), and thiophene (T) groups were selected as energy donor-acceptor-donor, acceptor, and donor-type chromophores to produce the expected three primary luminescent colors, red, green, and blue, respectively (Figure 1b). The synthetic details of Alk-TBT, Alk-B, and Alk-T can be found in the Experimental Section/Methods section. All compounds were unambiguously characterized by ^{1}H and ^{13}C NMR (Supplementary Information Figures S1–S11) and matrix-assisted laser desorption/ionization time-of-flight mass spectrometry (MALDI-TOF-MS) (Figures S12–S14). ^{1}H NMR also indicated the absence of residual solvents for all three compounds in the liquid state. The blending combination applied in this study is shown in Figure 1c.

According to the results of small- and wide-angle X-ray scattering (SWAXS) (Figure 2a), Alk-TBT, Alk-B, and Alk-T exhibit two halos, in which the halo in the smaller q region corresponds to the average distance (Alk-TBT: 21.6 Å, Alk-B: 21.5 Å, and Alk-T: 21.3 Å) between the π-core moiety of the adjacent molecules, while the other halo in the larger q region is attributable to the average spacing of the short-range distribution (around 4.6 Å) among molten alkyl chains. This is typical of alkyl-π liquids in SWAXS or X-ray diffraction (XRD) patterns [32,34,39,49,54,62]. In addition, the absence of birefringence under the observation of polarized optical microscopy (POM) illustrates no long-range ordering in the three liquids (Figure 2b). In the heating scan of differential scanning calorimetry (DSC; Figures 2c and S15), only a single glass transition (T_g) was observed for all three liquids (Alk-TBT: −54 °C, Alk-B: −59 °C, Alk-T: −61 °C), which are sufficiently lower than room temperature, indicating their liquid state at room temperature. According to the report, 2-octyldodecyl chains can construct superior liquids at the (2,5-) substitution position of the phenyl group [28,32,34]. The three liquids have been practically stable at room temperature for four years (since synthesis), and Figure S16 also shows that these liquids do not have supercooling behavior [63]. Thermogravimetry analysis (TGA; Figure S17) proves that the three liquids have relatively high thermal stability, and the thermal decomposition temperatures (5% weight loss, $T_{95\%}$) are up to 362 °C at least. These results indicate that their liquid state is practically stable within the wide temperature range of approximately – 50 °C to 350 °C.

2.2. Miscibility evaluation by general approaches

Miscibility refers to the ability of two or more components to mix thoroughly in any proportion without phase separation. Achieving a perfectly miscible blend is essential for high-quality color tuning, and evaluating miscibility is of critical importance. Common characterization methods for miscibility are primarily considered in terms of physical properties such as density, refractive index, and viscosity, as well as structural difference analysis by XRD and thermal analysis by DSC. The criterion is that when components with distinct physical properties are immiscible, their individual properties are retained. In contrast, if a miscible homogeneous phase forms after blending, a single intermediate property merges, reflecting a combination of the original components. As discussed earlier, the SWAXS results showed that the three liquids are amorphous with similar structural distance information, making it difficult to determine their miscibility by using SWAXS (or XRD). Another example of similar physical properties is the density

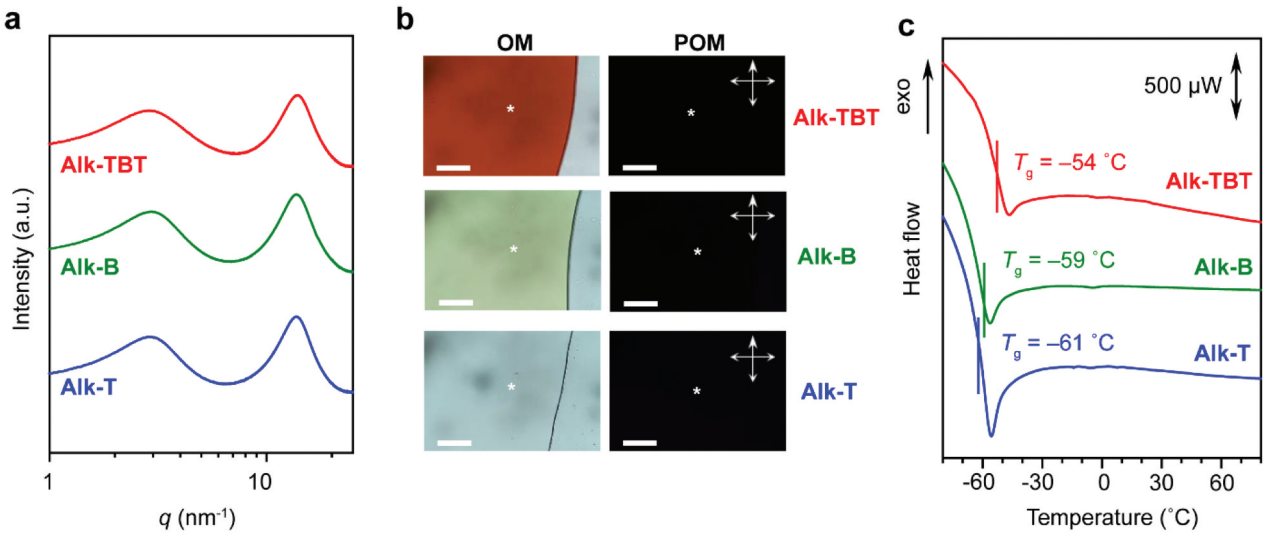

Figure 2. a) SWAXS profiles of Alk-TBT, Alk-B, and Alk-T at 23.0 ± 0.5 °C. (b) OM and POM images of Alk-TBT, Alk-B, and Alk-T were taken at 23.0 ± 0.5 °C. The region marked with an asterisk (*) represents the sample. Scale bar: 50 μm. c) DSC traces of Alk-TBT, Alk-B, and Alk-T during the heating scan at 10 °C min^{-1} under the nitrogen atmosphere.

(Alk-TBT: 0.93 g cm^{-3}, Alk-B: 0.91 g cm^{-3}, Alk-T: 0.91 g cm^{-3}). In this case, density could not be used as an indicator to evaluate miscibility for these liquids. Next, we attempted to assess the miscibility of the liquids using positron annihilation lifetime spectroscopy (PALS; Figure S18, Table S1) based on the fractional free volume [64–67] of the liquids, but a clear conclusion was not reached. As an additional evaluation method, we explored the possibility of measuring the refractive index (nD): the nD of Alk-TBT (1.578) was sufficiently different from that of Alk-B (1.513) and Alk-T (1.513) so that it could be used to determine the miscibility of Alk-TBT/Alk-B and Alk-TBT/Alk-T blends. With the increase in the content of one component, nD showed a linear increase (Figure S19a-b), allowing the evaluation of the high miscibility of Alk-TBT/Alk-B and Alk-TBT/Alk-T. In contrast, in the case of immiscible liquid blends, for example, a blend of hydrophilic molten polymer polyethylene glycol PEG (nD = 1.466) and hydrophobic liquid Alk-T (Alk-T/PEG), an irregular refractive index distribution was seen, hinting at the presence of phase separation (Figure S19c). However, this technique is not universal since the refractive indices of Alk-B and Alk-T are similar; thus, it is unable to judge the miscibility of Alk-B/Alk-T blends. DSC, a more versatile evaluation technique, was used to evaluate the miscibility of the liquids using the glass transition temperature (T_g) [62,68,69]. Multiple T_g values are usually recognized in blend systems where phase separation occurs. The DSC curves (Figure S20) of three binary blends (Alk-TBT/Alk-B, Alk-B/Alk-T, and Alk-TBT/Alk-T) and a ternary blend (Alk-TBT/Alk-B/Alk-T) were analyzed through DSC and DDSC signals. As a result, only a single T_g was observed for all blends. Generally, a single T_g for a blend is a miscible system. However, the individual T_g values of the three liquids are close (Figure 2c), so detecting the slight difference in T_g is difficult even if phase separation occurs. Therefore, the abovementioned methods are not fully applicable to this system, and other robust methods are needed to judge and evaluate the miscibility.

2.3. Miscibility evaluation by rheological analysis

The time – temperature superposition (TTS) [70] principle was employed for rheological analysis to characterize the liquid blending systems and discuss the miscibility. Rheological analysis [71] has several advantages: i) its broad scope of application means that it can be used to study almost any fluid without being limited by the chemical structure or properties; ii) the liquid sample testing process is nondestructive to the sample; and iii) the rheological response is sensitive enough to identify changes in the internal structure of the liquids.

In simple terms, regarding the viscoelastic behavior of a fluid, increasing the temperature is equivalent to extending the time, known as 'time – temperature equivalence'. According to this principle, the fluid's dynamic modulus curves at different temperatures are shifted using the shift factors and are superimposed on the reference temperature to form a rheological master curve at the reference temperature, which contains the key parameters horizontal shift factor α_T and vertical shift factor b_T. Miscibility can be confirmed by verifying the TTS principle: if phase separation occurs, the TTS principle is not satisfied [70]. For example, we performed rheological TTS analysis of a sample where Alk-TBT was blended with Alk-T to make 10 mol% (i.e. 10 mol% Alk-TBT/Alk-T). In the experiment, we measured the temperature-dependent rheology of the blend to obtain the storage (G') and loss (G'') moduli at different temperatures (Figure 3a). Taking 20 °C as the reference temperature, the moduli at each temperature were superimposed by horizontal and vertical shifts to generate two fully independent curves (Figure 3b), called rheological master curves. Two crucial parameters are α_T and b_T. α_T, which varies with the reference temperature, is obtained by shifting the curve. b_T, derived from the van Gurp – Palmen plot, is constant across temperatures, typically 1. With α_T, we can obtain the rheological master curve at any reference temperature, usually applying the Williams – Landel – Ferry (WLF) equation [70], which is an empirical equation expressed as:

$$\mathrm{Log}(\alpha_T) = \frac{-C_1 \cdot (T - T_0)}{C_2 + (T - T_0)} \quad (1)$$

where T_0 is the reference temperature, C_1 and C_2 are empirical parameters associated with T_0, and α_T is the horizontal shift factor [72]. Figure 3c shows the WLF curves of the binary blend Alk-TBT/Alk-T when T_0 is 20 °C. The primary function of the WLF equation and TTS is to enable rheological data measured at low temperatures to be extrapolated to short periods (or high frequencies). Alk-TBT, Alk-B, and Alk-T and their blends follow the TTS (Figures S21 and S22), allowing the prediction of the rheological behaviors using the WLF equation (Figure S23). The results suggest a high miscibility of the blends, as the absence of phase separation is generally considered an important condition for compliance with the TTS. For a more intuitive comparison, we evaluated the immiscible case to see what happens when TTS is not met. Figure S24a indicates the rheological results (dynamic frequency sweep) of the blend of 10 mol% PEG in Alk-T. The van Gurp – Palmen plot (Figure S24b) determines b_T (here, all b_T are 1), and Figure S24c is obtained by horizontal shifting. G'' was selected as an example. In the low-temperature region, the master curve of the PEG/Alk-T blends is almost the same as in

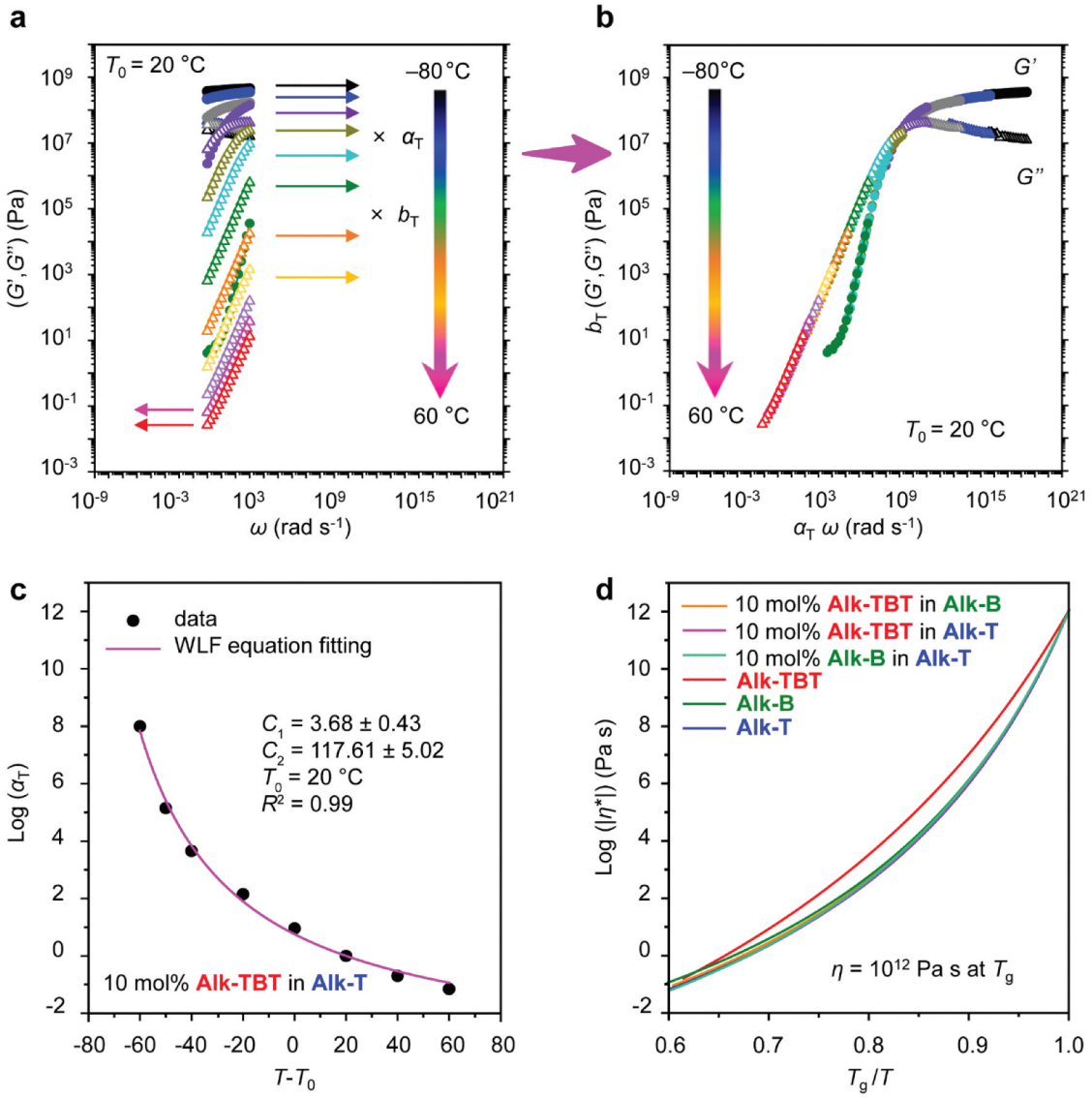

Figure 3. a) temperature dependence of rheological results of 10 mol% Alk-TBT in Alk-T blend. b) rheological master curves obtained by shifts at a reference temperature T_0 = 20 °C. c) WLF equation plot for 10 mol% Alk-TBT in Alk-T blend, T_0 = 20 °C. d) Angell plot of Alk-TBT, Alk-B, Alk-T and their blends (10 mol% Alk-TBT in Alk-B, 10 mol% Alk-TBT in Alk-T, and 10 mol% Alk-B in Alk-T).

the miscible case. Nevertheless, a significant modulus jump at high temperatures indicates that it is not a perfect curve and does not comply with the TTS. The PEG/Alk-T blend undergoes phase separation as the temperature increases. Figure S24a shows that G'' and G' intersect in the high-temperature region, indicating a phase change.

Activation energy (E_a) is a critical parameter representing the energy barrier that molecules must overcome to undergo molecular motions, making it essential for understanding molecular blending behavior. One method for deriving E_a is through its relationship with zero shear viscosity (η^0). In general, zero shear viscosity ($\eta^0 = \lim\ \omega{-}0\ |\eta^*|$) is the viscosity of a static fluid. It can be obtained for shear-thinning liquids by achieving a constant complex viscosity after shear thinning. For non-Newtonian fluids at extreme temperatures, TTS can extrapolate η^0 using the master curve. In the case of liquids Alk-TBT, Alk-B, and Alk-T, the details are summarized in Table S2. According to the Arrhenius equation, by plotting 1/T against η^0 or η^*, the corresponding molecular activation energy can be calculated (Figure S25). It should be noted that two values of E_a for the three liquids appeared in the higher and lower temperature regions around T_g (Table S3). E_a is rarely seen in the region below T_g. It is probably due to bulky but flexible alkyl side chains, which create the potential for configurational change even in the glassy state [72]. In the liquid state, the E_a values of Alk-TBT, Alk-B, and Alk-T were 86.3, 68.4, and 68.6 kJ mol^{-1}, respectively. The E_a of Alk-TBT is more significant than that of Alk-B and Alk-T, indicating that Alk-TBT is more sensitive to temperature changes than Alk-B and Alk-T. Furthermore, the E_a values of the three liquids are comparable to that of

Table 1. VFT parameters and fragility (m) determined from the viscosity.

	VFT parameters			
entry	$10^6 \times \eta_\infty$ [a]	D [b]	T_0 [c]	m [d]
Alk-TBT	0.0508	20.7	139.7	60.7
Alk-B	9.76	10.4	157.5	80.8
Alk-T	4.89	10.5	158.1	82.8
10 mol% Alk-TBT in Alk-B	5.36	10.7	158.5	81.2
10 mol% Alk-TBT in Alk-T	3.58	10.9	158.0	81.8
10 mol% Alk-B in Alk-T	2.61	11.4	156.6	81.4

[a]Viscosity at infinity temperature. [b]Stiffness. [c]Temperature where viscosity diverges to infinity. [d]Fragility.

the reported alkyl-π liquids (38.8–48.1 kJ mol^{-1} for alkyl – distyrylbenzene liquids [28] 62–77 kJ mol^{-1} for alkyl – C_{60} liquids [49]). E_a increased to more than 200 kJ mol^{-1} in the glassy state, which is about 2.5 to 4 times higher than in the liquid state. This is thought to be because molecular motion is suppressed in the glassy state compared to the liquid state [73]. The change in viscosity with the temperature in the glass transition region reflects the dynamic properties.

Angell et al. [74] proposed a theory of strong and fragile liquids. Strong liquids follow the Arrhenius equation, and behaviors that deviate from the Arrhenius equation can be fitted by the Vogel – Fulcher – Tammann (VFT) equation:

$$\eta(\mathrm{T}) = \eta_\infty \exp\left(\frac{DT_0}{T - T_0}\right) \quad (2)$$

where η_∞ represents the viscosity at an infinite temperature, D is the stiffness, and T_0 is the temperature where the viscosity diverges to infinity. Each of these is a constant. The degree of deviation is typically described by the fragility (m) [26,75].

$$m = \frac{\partial \log_{10}\eta(\mathrm{T})}{\partial\left(\frac{T}{T_g}\right)}\Big|_{T=T_g} \quad (3)$$

In the present system, individual liquids exhibit different m values: Alk-TBT: 60.7, Alk-B: 80.8, and Alk-T: 82.8 (Figure 3d, Table 1), indicating that Alk-TBT is the strongest liquid and Alk-T is the most fragile liquid among the three. On the contrary, the VFT relationship was maintained for all binary blends, and the m values were comparable to those of pure Alk-T and Alk-B. Therefore, these blend liquids have a similar fragility as the Alk-T or Alk-B liquid alone: a similar degree of heterogeneity in the amorphous molecular dynamics. This result also supports the miscibility between the alkyl-π liquids.

2.4. Multi luminescent color tuning

To verify the merge of π-functions of multiple types of alkyl π-liquids, fluorescence, a representative example of π-function, was used as a probe. By blending two or three types of alkyl π-liquids that luminescent red (Alk-TBT), green (Alk-B), and blue (Alk-T) light, respectively, we demonstrate a system in which the luminescent color can be precisely and uniformly controlled to the desired color.

To understand the optical properties of Alk-TBT, Alk-B, and Alk-T, UV-Vis absorption and fluorescence spectroscopies in different solvents and the solvent-free liquid state were measured (Figure 4a). The UV-Vis absorption and fluorescence spectra of Alk-B and Alk-T are almost identical in dilute toluene solution and in the liquid state, which means that in the solvent-free liquid state, the π-cores of adjacent molecules are sufficiently separated by the branched alkyl chains that are arranged around the π-cores. Figure 1b shows that Alk-TBT, Alk-B, and Alk-T in the liquid state under 365 nm UV light irradiation exhibit red, green, and blue fluorescence with an absolute fluorescence quantum yield (Φ_{FL}; Table S4) of 0.65, 0.74, and 0.14, respectively. The higher Φ_{FL} of Alk-TBT and Alk-B can be explained by the definition of the absolute fluorescence quantum yield. The Φ_{FL} is defined as:

$$\Phi_{FL} = \frac{k_R}{k_R + k_{NR}} \quad (4)$$

where k_R represents the radiative decay rate constant, and k_{NR} is the nonradiative decay rate constant. The k_{NR} of Alk-T is high both in toluene and in the liquid state (Table S4), almost two orders of magnitude higher than Alk-TBT and Alk-B. As a result, the loss of nonradiative energy directly translates into a decrease in Φ_{FL}. The CIE 1931 chromaticity diagram is often adopted to better evaluate colors. The luminescent color coordinates of Alk-TBT, Alk-B, and Alk-T in the liquid state (Alk-TBT: (0.64, 0.36), Alk-B: (0.30, 0.54), Alk-T: (0.17, 0.09)) are close to the standard color coordinates: (sRGB): sR (0.64, 0.33), sG (0.30, 0.60), and sB (0.15, 0.06) (Figure 4b). The homogeneous blending of the three liquids will result in a multi-color system with uniform luminescent colors. In this study, Alk-T acts as the energy donor, Alk-TBT acts as the energy acceptor, and Alk-B sits in between. The role of Alk-B changes to energy donor or acceptor depending on what is blended. The large area that overlaps between the donor fluorescence spectrum and the acceptor absorption spectrum (Figure S26) suggests that blending any two components

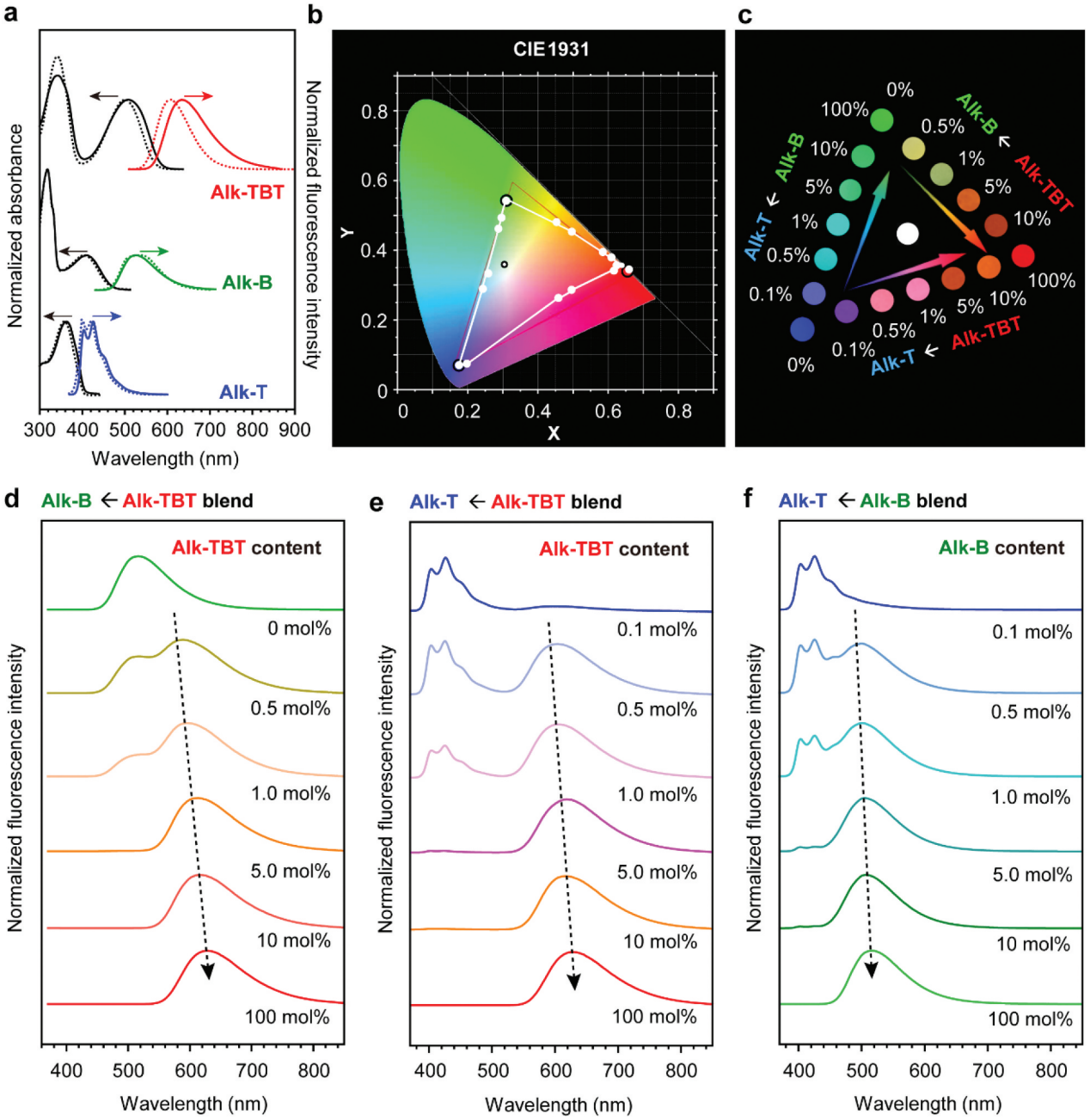

Figure 4. A) UV-Vis absorption and fluorescence spectra of Alk-TBT, Alk-B, and Alk-T in a solvent-free liquid state (solid line) and in dilute toluene solution (dotted line), 10^{-5} mol L^{-1} for absorption and 10^{-6} mol L^{-1} for fluorescence measurement. Two absorption peaks appeared for Alk-TBT and Alk-B, and normalization was performed based on the peak at a longer wavelength. The direction indicated by the arrow is the corresponding absorption or fluorescence spectrum. b) fluorescent color distribution of binary/ternary blends on CIE 1931 chromaticity diagram. c) color change diagram of binary/ternary blends (corresponding CIE 1931 chromaticity diagram). The white color coordinate (0.30, 0.33) was obtained with Alk-TBT/Alk-B/Alk-T ratio of 0.05/0.30/100. d-f) fluorescence spectral changes of the binary blends are shown in a stacked mode.

facilitates the occurrence of FRET from Alk-T to Alk-B, Alk-T to Alk-TBT, and Alk-B to Alk-TBT. The change in the blends' luminescent color directly reflects this phenomenon. Fine-tuning of the luminescent color is easily achievable for binary and ternary liquid blends by adjusting the ratio of donor to acceptor.

As typical examples, the luminescent color coordinates and distributions of three binary blend combinations are shown in Figure 4b. The excitation spectra of the binary and ternary blends (Figure S27) indicate that the excited donor (Alk-T or Alk-B) contributes to the fluorescence of the acceptor (Alk-TBT or Alk-B). The Φ_{FL} of the binary blends (Table S5-S7) also reflects the occurrence of efficient FRET, as a moderate increase in the acceptor content leads to an overall enhancement in Φ_{FL}. The luminescent color of the blend of two liquids is distributed on the connecting line of the luminescent colors of each liquid. With increasing acceptor component, the luminescent color gradually transitions toward the acceptor-dominated emission (Figure 4c). In all cases, increasing the

acceptor component leads to a gradual red shift in its fluorescence (Figure 4d–f, indicated by dashed arrows). Reabsorption may contribute to the observed red-shift, as its complete elimination is highly impractical in the solvent-free state. At higher acceptor concentrations, reabsorption becomes more pronounced, as its emission in a spectral region where absorption is inherently present, particularly at the shorter wavelengths. As will be shown later, Alk-B and Alk-TBT exhibit relatively strong solvatochromic effects. Even in the absence of an external solvent, the donor and acceptor, both being in the liquid state, act as the solvent. At low acceptor concentrations, the donor primarily acts as the solvent, solvating the acceptor molecules. With increasing acceptor component, self-solvation by the acceptor itself becomes more dominant. This progressive change in the solvation environment modifies the overall polarity of the system, leading to a solvatochromic-like effect that enhances emission at longer wavelengths.

We emphasize that adding a minute amount of the acceptor component leads to a significant change in the luminescent color, resulting in a high efficiency of FRET (Φ_{FRET}). For instance, in Alk-TBT/Alk-T blends, the fluorescence spectra of Alk-TBT and Alk-T can be clearly resolved and separately integrated (Figure S28a, b) so that Φ_{FL} of each blend can be obtained by calculation, and the following formula can obtain Φ_{FRET} [76]:

$$\Phi_{FRET} = \frac{1-\Phi_{FD}}{\Phi_{FD0}} \quad (5)$$

where Φ_{FD} is the quantum yield of the donor component in the blend, and Φ_{FD0} corresponds to the value without the donor liquid. Consequently, by blending only 0.1 mol% of Alk-TBT in Alk-T, Φ_{FRET} increased to 37.8%. Remarkably, by increasing the ratio to 5 mol%, Φ_{FRET} reached an unprecedented value of 97%, almost approaching 100%. Some reports [77] suggest that donors with higher energy levels can rapidly promote efficient FRET. However, in the present system, the Φ_{FL} of the blue-emitting liquid donor (Alk-T) was only 0.14. Even when the liquid acceptor content increased from 0 to 5 mol%, the Φ_{FL} of Alk-T decreased by only 0.091, from 0.14 to 0.049, and nearly 100% FRET was achieved (Figure S28c). This intriguing result suggests that efficient FRET can be achieved by homogeneously blending a low-energy liquid donor with a high-energy liquid acceptor. Implementing ternary blends was essential to attain broad tuning, particularly for exploring white-emission conditions.

We started by searching for Alk-TBT/Alk-T ratios of 1/100 and 0.5/100 and then further adjusted the Alk-TBT/Alk-T ratio to obtain four ratio combinations. A comparison with the CIE 1931 chromaticity diagram (Figures S29 and S30) revealed that fine-tuning was necessary to reduce the green component properly. When the Alk-TBT/Alk-B/Alk-T ratio was 0.05/0.30/100, the white color coordinate (0.30, 0.33) [78] was obtained, which is very close to the standard white light color (Figures 4b,c). For reference, the fluorescence and excitation spectra are displayed in Figure S31. Therefore, wide-range luminescence color can be achieved by tuning the binary and ternary liquid blending ratios. The prerequisites for achieving the targeted tuning of luminescent colors are homogeneous liquid blending and the occurrence of FRET, which has been successfully demonstrated in this system.

To further verify the effectiveness of this strategy, we performed a study blending Alk-T with the reference solid sample Me-B (Supplementary Information, Figures S10–S11). Me-B is a solid fluorophore with the same chromophore as Alk-B, except that the branched alkyl side chains of Alk-B are replaced with methyl groups. Based on the Alk-B/Alk-T liquid blend mentioned above, we can infer that FRET also occurs between Me-B and Alk-T. When the acceptor Me-B (0.1 mol%) was added to the donor liquid matrix Alk-T, the fluorescence peak intensity of Alk-T began to decrease (Figure S32a). Meanwhile, a new luminescent peak appeared in the 500–550 nm region, which was evidence of the FRET occurrence phenomenon. Moreover, as the Me-B content increased (0.5, 1.0, 5.0 mol%), the fluorescence peak intensity of Alk-T gradually decreased. However, when the Me-B content was increased to 10 mol%, the fluorescence peak intensity of Alk-T decreased sharply, and the luminescent peak at 530 nm showed a slight red shift. This is most likely due to the severe aggregation of high concentrations of Me-B in Alk-T, and the OM/POM observations support this hypothesis. When the Me-B content is low at the initial blending stage, Me-B is slightly soluble in Alk-T, and the expected FRET behavior can be observed. However, with the increase in the amount of Me-B added, the solubility of Me-B in Alk-T was not high, so Me-B gradually aggregated and precipitated, resulting in solid – liquid phase separation. When the amount of Me-B added was 5 mol%, slight crystallization of Me-B was recognized in OM, and a weak birefringent texture was observed in POM (Figure S32b). When the amount of Me-B added was increased to 10 mol%, the Me-B aggregation-derived characteristics seen in OM/POM became more pronounced. Furthermore, crystallization was visible to the naked eye when the 10 mol% Me-B/Alk-T blend was left for one day at room temperature. This result suggests that the compatibility of solid dyes in alkyl-π liquids is limited to low concentration ranges. As the concentration of added solids increases, the solid dyes aggregate and precipitate, separating the solid – liquid phase.

The videos (Supplementary Videos 1 and 2) and Figure S33 visualize the difference between solid – liquid and liquid – liquid blending. When a small amount of green luminescent solid Me-B was placed on the surface of blue luminescent Alk-T, no significant color change was observed over time, i.e. Me-B was not dissolved in Alk-T, except for a lump of Me-B floating at the edge of the Alk-T surface. In contrast, when a liquid droplet of green luminescent Alk-B was placed on the Alk-T liquid surface, Alk-B rapidly diffused within Alk-T due to the flow properties of the liquid, forming a homogeneous and stable mixed phase. The results have demonstrated that alkyl-π liquid blends with excellent miscibility and homogeneity have been obtained, highlighting the advantages of liquid – liquid blending.

So, what is the function of each alkyl-π liquid as a medium? It is not easy to imagine that it is precisely the same as a nonpolar environment such as *n*-hexane, and it cannot be denied that it may provide a somewhat polar liquid medium environment depending on the π-conjugated core unit. In the Alk-B/Alk-T binary liquid blend, the luminescent color coordinates were linearly distributed along the line connecting the luminescent color coordinates of the two liquids (Figure 3b). However, the coordinates of the Alk-TBT/Alk-B and Alk-TBT/Alk-T blends deviated slightly from the linear distribution and cannot be ignored (Figure 3b). This is thought to be due to the polar effect caused by the π-conjugated core of the alkyl-π liquids. Different π-cores in Alk-TBT, Alk-B, and Alk-T should lead to varying polarities for the molecules. Interestingly, the liquid blends (Alk-TBT + Alk-B + Alk-T) can be separated by silica gel column chromatography, reflecting the mismatch of the three polarities (Figure S34 for photographs of the thin layer chromatography and silica gel column chromatography). In contrast, as mentioned earlier, a trace amount of acceptor liquid blended with a donor liquid achieves highly efficient FRET. Therefore, the donor liquid plays the role of a host medium in such blends and is responsible for the effect of the 'solvent'. Further investigations on the solvatochromic impact of the liquid blend system should be useful for gaining a deeper understanding of the deviations seen in the blends (Alk-TBT/Alk-B and Alk-TBT/Alk-T).

Solvent-dependent UV-Vis absorption and fluorescence spectroscopies of Alk-TBT, Alk-B, and Alk-T were performed with *n*-hexane, toluene, tetrahydrofuran (THF), chloroform ($CHCl_3$), and dichloromethane (CH_2Cl_2). In the UV-Vis absorption spectra (Figure 5a), polarity was insensitive for the three compounds. With increasing solvent polarity, Alk-TBT and Alk-B showed corresponding shifts in their

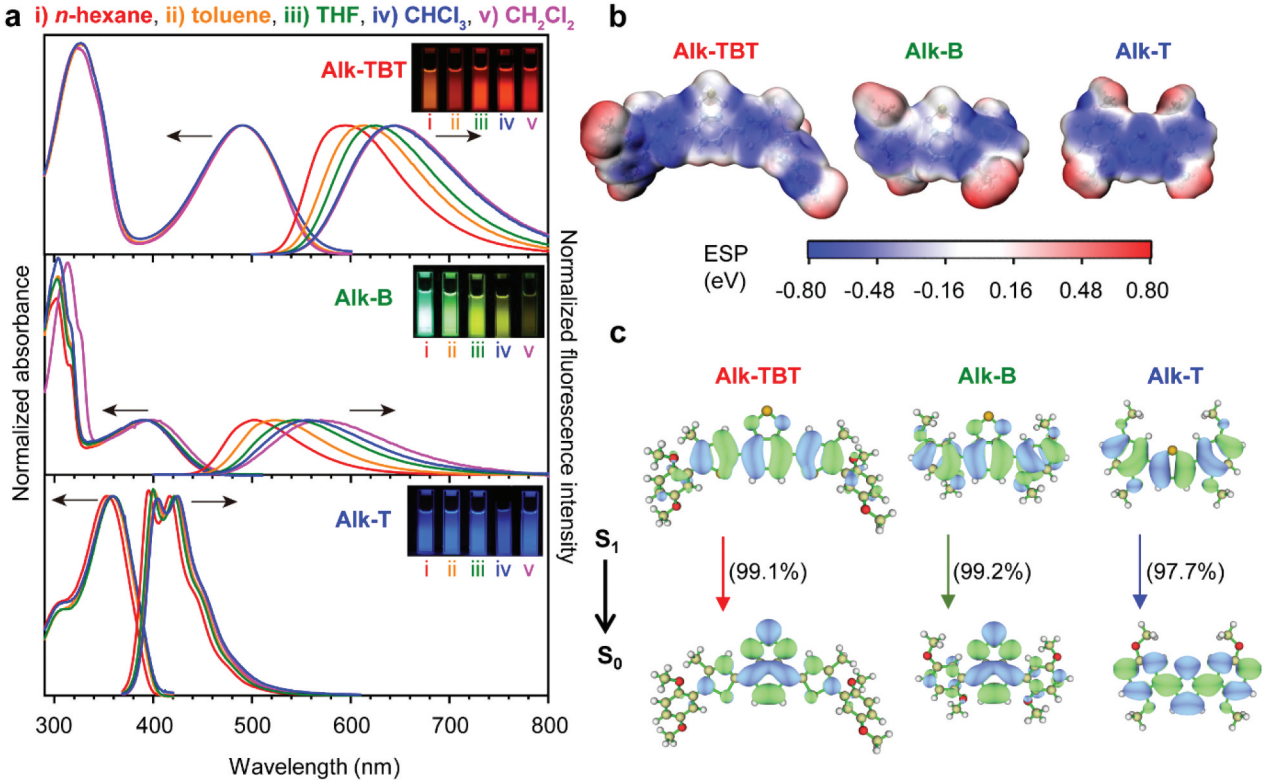

Figure 5. A) UV-Vis absorption and fluorescent spectra of Alk-TBT, Alk-B, and Alk-T in solvents, e.g. i) *n*-hexane, ii) toluene, iii) THF, iv) $CHCl_3$, and v) CH_2Cl_2 of different polarities. Inset photographs in figure 5a, taken under 365 nm UV light irradiation, correspond to the polarity of the solutions from small i) *n*-hexane to large v) CH_2Cl_2. The direction indicated by the arrow is the corresponding spectrum. Two absorption peaks appeared for Alk-TBT and alk-B, and normalization was performed based on the peak at a longer wavelength. b) electrostatic potential distributions of alk-TBT, alk-B, and alk-T in excited states. c) natural transition orbitals of S_1 and S_0 states for Alk-TBT, Alk-B, and Alk-T.

fluorescence spectra, while Alk-T showed little change. The wavelengths of the maximum emission peaks for Alk-TBT and Alk-B red-shifted by 50 nm (from 595 to 645 nm) and 66 nm (from 504 to 570 nm), respectively, in solvents ranging from a nonpolar *n*-hexane to a polar CH_2Cl_2. Under the same solvent conditions, Alk-T shifted by only 7 nm (from 417 to 424 nm). Theoretical calculations [79] were conducted to explore the origins behind the solvatochromic effect.

Based on the B3LYP functional of the density functional theory (DFT), geometric optimization of the ground state of the target molecule (a simplified model in which branched alkyl chains are replaced with methyl groups) was performed using the 6-31 G (d,p) basis set, and the structure was optimized by frequency analysis. No imaginary frequencies were present, confirming that the optimized structure was at the lowest energy point on the potential energy surface. The simplified model of the ground state/excited states of Alk-TBT, Alk-B, and Alk-T was calculated at the CAM-B3LYP/6-31 G(d,p) level of theory. The polarizable continuum model (PCM) was used to model the solvatochromic phenomenon, in which *n*-hexane and CH_2Cl_2 were selected as representatives of low- and high-polarity solvents. All calculations were completed using the Gaussian program [80]. Electrostatic potential (ESP) and natural transition orbitals (NTOs) were analyzed with Multiwfn [81,82], and visualized via the Visual Molecular Dynamics (VMD) [83] program. It was speculated that one of the reasons for the solvatochromic effect was the charge redistribution caused by electron excitation, the root cause of which was the change in the dipole moment. The calculation results are summarized in Table 2. Suppose the dipole moments of the three molecules in the first excited state are more significant than those in the ground state. In that case, the interactions between the solvent and solute molecules also become more important than those between the molecules in the ground state. The excited state dipole moment and solute/solvent intermolecular forces increase with an increase in the solvent polarity. The fluorescence generation of the three molecules is due to the orbital transition of electrons from the lowest unoccupied molecular orbital (S_1) to the highest occupied molecular orbital (S_0), and their energy band gap (ΔE) affects the difficulty of the transition. Notably, the ΔE of the excited states Alk-TBT and Alk-B is smaller than that of Alk-T, whether in the solvent or the gas phase. This indicates that Alk-TBT and Alk-B are more likely to undergo electronic transitions. This also explains why a solvatochromic effect was not observed in Alk-T. In addition, the theoretically calculated values of the emission maximum wavelength were consistent with the experimental values (Table 3), which fully indicates the influence of the solvatochromic effect on Alk-TBT and Alk-B. Alternatively, the molecular electrostatic potential and natural transition orbitals [79] can also explain the solvatochromic effect.

Figure 5b shows the surface electrostatic potential distribution diagram of three simplified molecules in the excited state. The methoxy groups attached to the 2,5-position of the phenyl group exhibit a relatively large positive potential due to the presence of the methyl groups. At the same time, non-alkyl moieties exhibit negative potential. Such a nonuniform electrostatic potential distribution facilitates interactions with polar molecules. The analysis of natural transition orbitals further supported this conclusion. Figure 5c shows the natural transition orbital pairs from S_1 to S_0 for the three compounds in the gas phase. The phenyl units in Alk-TBT and Alk-B tend to form electron-deficient structures, whereas Alk-T is not in a similar situation. Moreover, the transition tendency weights of all three compounds exceeded 97%. Therefore, the solvatochromic effect in Alk-

Table 2. The dipole moments and energy band gaps from different states.

	Alk-TBT		Alk-B		Alk-T	
	dipole moment (Debye)	ΔE (eV)	dipole moment (Debye)	ΔE (eV)	dipole moment (Debye)	ΔE (eV)
ground state (gas-phase)	1.14	4.86	1.85	5.47	1.02	6.11
excited state (gas-phase)	4.81	4.15	5.69	4.67	2.02	5.23
excited state (in *n*-hexane)	5.11	4.11	6.38	4.63	2.60	5.19
excited state (in CH_2Cl_2)	5.42	4.13	7.43	4.65	2.67	5.14

Table 3. Comparison of the maximum wavelengths of fluorescence for three liquids in different states.

	Alk-TBT		Alk-B		Alk-T	
	theoretical value (nm)	actual value (nm)	theoretical value (nm)	actual value (nm)	theoretical value (nm)	actual value (nm)
solvent-free state	576	626	488	516	399	425
in *n*-hexane	595	595	500	504	417	417
in CH_2Cl_2	625	645	515	570	442	424

TBT and Alk-B can be explained by the change in the dipole moment at the excited state and the inhomogeneity of the electrostatic potential distribution, as well as the analysis of the natural transition orbitals. In summary, the difference in polarity of the liquid itself is the main factor leading to the slightly deviated color distribution of the blended system.

3. Conclusion

To manage and regulate the π-functions of alkyl π-liquids, it is advisable to avoid the labor-intensive chemical synthesis of individual and distinct liquid molecules, as well as the inconsistencies and unreliability of their properties associated with the use of solid dopants. To address this challenge, we have devised a liquid-liquid blending strategy. Phase separation was not observed in the highly miscible liquid blends, even at an equimolar blending ratio (Figure S35) while employing this technique. In certain instances, the linear distribution of the refractive index exhibited miscibility; however, this phenomenon is not universally applicable to all liquid blends. Comparing the miscibility with liquid – liquid and solid – liquid blends confirmed the many advantages associated with miscibility for alkyl-π liquid blends. It is important to note that rotational rheology serves as the most effective measurement technique for verifying the miscibility and homogeneity of liquid – liquid blends. Photoluminescent color tuning is comprehensively demonstrated as an exemplary illustration of the merging π-functions. Using binary and ternary liquid blends equipped with energy donor and acceptor functions has resulted in efficient FRET-induced luminescent color shifts. Additionally, these blends exhibit extensive control over luminescence color, attributable to their uniform compatibility. One caveat of this approach is that the environment in alkyl-π liquids may act as a moderately polar medium. As anticipated by the theoretical model, the luminescent color distributions of binary blends showed slight deviations from a linear progression in color distribution, attributed to the polarity of the π-conjugated cores of Alk-TBT and Alk-B. The liquid – liquid blending method implemented in this study for alkyl-π liquids facilitates the production of low-volatility, ink-like materials that exhibit a diverse spectrum of uniform luminescent colors, devoid of any color unevenness. Furthermore, by capitalizing on the softness and fluidity of the liquid, alkyl-π liquids and their liquid – liquid blends are expected to advance the development of light-emitting materials with high dimensional freedom, including flexible and flowable light-emitting devices [56,57]. The liquid – liquid blending method is anticipated to effectively merge and hybridize π-functions beyond luminescent color, paving the way for further advancements in liquid science.

4. Experimental section/methods

4.1. General materials

Carbon tetrabromide, 2,1,3-benzothiadiazole-4,7-bis (boronic acid pinacol ester), 2,5-bis(trimethylstannyl) thiophene, triphenylphosphine, potassium carbonate, and methyl trioctyl ammonium chloride were purchased from Sahn Chemical Technology Co., Ltd. (Shanghai, China), 2-octyl dodecanol and 4,7-bis(2-trimethylstannyl-4-hexyl-2-thienyl)-2,1,3-benzothiadiazole were obtained from Alfa Chemical Co., Ltd. (Zhengzhou, China), tetrakis(triphenylphosphine)palladium, tris-(dibenzylideneacetone)dipalladium(0) and tri(*o*-tolyl) phosphine were obtained from Greenchem Technology Co., Ltd. (Beijing, China). Bromohydroquinone was purchased from Tokyo Chemical Industry Co., Ltd. (Tokyo, Japan). All solvents used for the reactions, such as dichloromethane, *N,N*-dimethylformamide, chlorobenzene, and toluene, were sourced from Sahn Chemical Technology Co., Ltd. (Shanghai, China).

4.2. General synthetic methods

Three-step reactions synthesized the target compounds (Scheme S1). In the first step, 9-(bromomethyl)nonadecane underwent the Appel reaction. In the second step, 9(bromomethyl)nonadecane and bromohydroquinone underwent the Williamson reaction to obtain 1-bromo-2,5-bis (2-octyldodecyloxy)benzene. In the final step, the three target compounds were synthesized by either Suzuki or Stille coupling with different π-unit molecules. All calculations of the blending experiments in this study were based on molar ratios. All blending experiments were carried out by preparing the corresponding solutions, mixing them, and removing the solvent. Binary or ternary blends were separated by silica gel column chromatography, with the eluent being *n*-hexane: CH_2Cl_2 = 10:1.

4.3. General characterization methods

^1H and ^{13}C NMR spectra were tested by a Bruker AVANCE III 600 MHz superconducting nuclear magnetic resonance spectrometer (Bruker Corporation, Germany) or a JEOL ECZ 400S spectrometer (JEOL Ltd. Japan) at room temperature in $CDCl_3$. Chemical shifts are expressed in part per million (ppm, δ scale) and are referenced to tetramethylsilane (TMS). A Shimadzu AXIMA-CFR Plus station (Shimadzu Corporation, Japan) measured the matrix-assisted

laser desorption ionization time-of-flight mass spectra (MALDI-TOF MS). The measuring methods included linear positive (LP) and reflectron positive (RP) modes without matrix suppression. The measurements involved in this work were in RP mode. Thermogravimetric analysis (TGA) was performed with a TA Instruments SDT Q600 (TA Instruments, USA) under nitrogen flow at a heating rate of 10 °C min^{-1}. Differential scanning calorimetry (DSC) was performed using a Hitachi DSC7000X (Hitachi High-Tech Corporation, Japan) with a liquid nitrogen cooling accessory under nitrogen flow (25 mL min^{-1}). Small- and wide-angle X-ray scattering (SWAXS) measurements were performed using an Anton Paar SAXSess mc2 system (Anton Paar GmbH, Austria). Polarizing optical microscopy (POM) and optical microscopy (OM) images were performed using an optical microscope (Olympus BX51, Olympus Corporation, Japan) equipped with a CCD camera. UV-Vis absorption spectra were measured on an Thermo Fisher Evolution 220 (Thermo Fisher Scientific Inc., USA) or a JASCO V-770 spectrophotometer (JASCO Corporation, Japan). Fluorescence spectra were obtained on a Jasco FP-8300 spectrophotometer (JASCO Corporation, Japan). Absolute fluorescence quantum yields (Φ_{FL}) were recorded on a Hamamatsu Photonics Quantaurus C11347 (Hamamatsu Photonics K.K., Japan). Density measurements were performed with a Micromeritics AccuPyc II 1340 (Micromeritics Instrument Corporation, USA), using a 1.0 cm^3 inner cell. The refractive indices were measured by a KEM Kyoto Electronics RA-600 refractometer (Kyoto Electronics Manufacturing Co. Ltd., Japan). The Toyo Seiko PSA L-II system (Toyo Seiko Co., Ltd., Japan) was used for the positron annihilation lifetime spectroscopy (PALS). Rheology was performed by an Anton Paar MCR 702 rheometer (Anton Paar GmbH, Austria) equipped with a parallel plate geometry plate of a Peltier temperature controller. The measurement content includes the temperature dependence of the dynamic frequency sweep (DFS).

4.4. Synthesis steps and structure characterization

Alk-TBT; 4,7-Bis(2-trimethylstannyl-4-hexyl-2-thienyl)-2,1,3-benzothiadiazole (1.00 eq, 0.99 g, 1.26 mmol), S2 (2.20 eq, 2.0 g, 2.76 mmol), tri(*o*-tolyl)phosphine (0.25 eq, 0.095 g, 0.310 mmol), and tri-(dibenzylideneacetone)dipalladium(0) (0.05 eq, 0.057 g, 0.063 mmol) were placed in a two-necked flask. The air in the flask was replaced with nitrogen several times to provide a nitrogen atmosphere for the substrate. Anhydrous chlorobenzene (5.0 mL) was then added via a syringe. The mixture was heated to 120 °C, and the reaction was monitored by TLC. After the reaction was completed, the mixture was extracted with CH_2Cl_2/H_2O (×3), and the lower organic phase was collected. The product was purified by silica gel column chromatography with the eluent (CH_2Cl_2: *n*-hexane = 1:30) to afford a red liquid (1.39 g, 62% yield).

T_g (DSC): −54 °C. $T_{95\%}$ (TGA): 398 °C. ^{1}H NMR ($CDCl_3$, 400 MHz, TMS, r. t.): δ/ppm 0.81–0.89 (m, 30 H, $-CH_3$), 1.14–1.34 (m, 144 H, alkyl), 1.75–1.79 (m, 4 H, alkyl), 2.59 (t, J = 8.0 Hz, 4 H, alkyl), 3.76 (d, J = 5.5 Hz, 4 H, –O – CH_2–), 3.81 (d, J = 5.7 Hz, 4 H, –O – CH_2–), 6.88 (dd, J_1 = 9.0 Hz, J_2 = 2.8 Hz, 2 H, benzene), 6.90 (d, J = 4.7 Hz, 2 H, benzene), 6.93 (d, J = 3.0 Hz, 2 H, benzene), 7.83 (s, 2 H, thiophene), 8.05 (s, 2 h, benzene). ^{13}C NMR ($CDCl_3$, 150 MHz, TMS, r. t.): δ/ppm 14.02, 22.62, 26.81, 29.14, 29.30, 29.58, 30.00, 30.04, 30.60, 31.31, 31.39, 31.64, 31.86, 38.00, 38.09, 71.63, 72.65, 114.43, 115.31, 118.08, 124.49, 125.69, 128.93, 135.30, 137.36, 141.40, 151.25, 152.64, 153.03. MALDI-TOF MS (matrix: dithranol) calculated for $C_{118}H_{200}N_2O_4S_3$: 1806.47, found: 1806.85 [M]+.

Alk-B; 2,1,3-Benzothiadiazole-4,7-bis(boronic acid pinacol ester) (1.00 eq, 0.813 g, 2.10 mmol), **S2** (2.20 eq, 3.46 g, 4.61 mmol), potassium carbonate (10.0 eq, 2.90 g, 20.9 mmol), tetrakis(triphenylphosphine)palladium (0) (0.03 eq, 0.072 g, 0.062 mmol) and one drop of methyl trioctyl ammonium chloride were placed in a two-necked flask. The air in the flask was replaced with nitrogen several times to provide a nitrogen atmosphere for the substrate. Toluene (5.0 mL) and distilled water (1.0 mL) were then added via a syringe. The mixture was heated to 120 °C, and the reaction was monitored by TLC. After the reaction was completed, the mixture was extracted with CH_2Cl_2/H_2O, and the lower organic phase was collected. The crude product was purified via silica gel column chromatography (CH_2Cl_2:*n*-hexane = 1:8) and subsequent recycling HPLC with chloroform as the solvent to give Alk-B as a yellow-green liquid (2.02 g, 58% yield).

T_g (DSC): −59 °C. $T_{95\%}$ (TGA): 395 °C. ^{1}H NMR ($CDCl_3$, 400 MHz, TMS, r. t.): δ/ppm 0.82–0.88 (m, 24 H, $-CH_3$), 1.08–1.80 (m, 132 H, alkyl), 3.75 (d, J = 5.4 Hz, 4 H, –O – CH_2–), 3.8 (d, J = 5.7 Hz, 4 H, –OCH_2–), 6.91 (dd, J_1 = 3.0 Hz, J_2 = 9.0 Hz, 2 H, benzene), 6.98 (d, J = 9.0 Hz, 2 H, benzene), 7.14 (d, J = 3.0 Hz, 2 H, benzene), 7.68 (s, 2 H, benzene). ^{13}C NMR ($CDCl_3$, 150 MHz, TMS, r. t.): δ/ppm 14.11, 26.69, 26.87, 29.32, 29.35, 29.58, 29.61, 29.64, 29.66, 29.69, 29.99, 30.06, 31.27, 31.37, 31.88, 31.93, 71.51, 71.92, 114.25, 114.96, 118.04, 127.84, 129.64, 130.72, 150.86, 153.22, 154.1. MALDI-TOF MS (matrix: dithranol) calculated for $C_{98}H_{172}N_2O_4S$: 1473.30, found: 1474.92 [M]+.

Alk-T; 2,5-Bis(trimethylstannyl)thiophene (1.00 eq, 1.00 g, 2.45 mmol), **S2** (2.20 eq, 4.03 g, 5.38 mmol), tri (*o*-tolyl)phosphine (0.25 eq, 0.186 g, 0.611 mmol) and

tri(dibenzylideneacetone)dipalladium(0) (0.05 eq, 0.111 g, 0.122 mmol) were placed in a two-necked flask. The air in the flask was replaced with nitrogen several times to provide a nitrogen atmosphere for the substrate. Anhydrous chlorobenzene (5.0 mL) was then added via a syringe. The mixture was heated to 120 °C, and the reaction was monitored by TLC. After the reaction was completed, the mixture was extracted with CH_2Cl_2/H_2O, and the lower organic phase was collected. The product was purified by silica gel column chromatography with the eluent (CH_2Cl_2:*n*-hexane = 1:30) to afford a light green liquid (2.14 g, 58% yield).

T_g (DSC): −61 °C. $T_{95\%}$ (TGA): 375 °C. ^{1}H NMR ($CDCl_3$, 400 MHz, TMS, r. t.): δ/ppm 0.84–0.90 (m, 24 H, $-CH_3$), 1.23–1.46 (m, 128 H, alkyl), 1.77–1.89 (m, 48 H, alkyl), 3.87 (d, J = 5.6 hz, 4 H, $-O-CH_2-$), 3.90 (d, J = 5.5 hz, 4 H, $-O-CH_2-$), 6.77 (dd, J_1 = 3.0 Hz, J_2 = 8.8 Hz, 2 H, benzene), 6.89 (d, J = 9.0 Hz, 2 H, benzene), 7.23 (d, J = 3.0 Hz, 2 H, benzene), 7.51 (s, 2 H, thiophene). ^{13}C NMR ($CDCl_3$, 150 MHz, TMS, r. t.): δ/ppm 14.11, 22.68, 26.89, 29.35, 29.63, 29.66, 30.07, 31.38, 31.50, 31.92, 38.13, 71.50, 72.16, 113.69, 113.89, 114.38, 124.39, 125.90, 139.15, 149.80, 153.32. MALDI-TOF MS (matrix: dithranol) calculated for $C_{96}H_{172}O_4S$: 1422.30, found: 1422.59 [M]+.

Disclosure statement

No potential conflict of interest was reported by the author(s).

Funding

This work was supported by Japan Society for the Promotion of Science KAKENHI Grant Number JP24H01733 and JP25H01264 in a Grant-in-Aid for Transformative Research Areas “Materials Science of Meso-Hierarchy” and “π-Molecular Complexity”, respectively, and National Natural Science Foundation of China (grant no. 52173175). We acknowledge the World Premier International Research Center Initiative (WPI), MEXT, Japan. Z. G. acknowledges the NIMS Junior Researcher fellowship for the Hokkaido University-NIMS Joint Graduate School Program. We thank Dr. Kazuhiko Nagura (NIMS) for the insightful discussion.

ORCID

Zhenfeng Guo http://orcid.org/0000-0001-6024-9703
Chengjun Pan http://orcid.org/0000-0001-9911-2966
Akira Shinohara http://orcid.org/0000-0002-7917-8092
Takashi Nakanishi http://orcid.org/0000-0002-8744-782X

Author contribution

T.N. and C.P. designed the project and supervised and edited the manuscript. Z.G. synthesized the compounds, performed and analyzed all experiments, and wrote the manuscript. A.S. participated in analysis and discussions. All authors have approved the final version of the manuscript.

Data availability statement

Raw data were generated at the National Institute for Materials Science. Derived data supporting the findings of this study are available from the corresponding author, T.N., on request.

References

[1] Tang S-Y, Mitchell DRG, Zhao Q, et al. Phase separation in liquid metal nanoparticles. Matter. 2019;1(1):192–204. doi: 10.1016/j.matt.2019.03.001
[2] Akada M, Toshinari H, Junji T, et al. Superconductivity appearing from C_{60} doped with rare-earth metals. Sci Technol Adv Mater. 2006;7(sup1):S83–S87. doi: 10.1016/j.stam.2006.03.005
[3] Mrđenović D, Abbott D, Mougel V, et al. Visualizing surface phase separation in PS-PMMA polymer blends at the nanoscale. ACS Appl Mater Interfaces. 2022;14(21):24938–24945. doi: 10.1021/acsami.2c03857
[4] Chen CY, Yunus WMZW, Chiu HW, et al. Phase separation behaviour in blends of isotactic polypropylene and ethylene–propylene diene terpolymer. Polymer. 1997;38(17):4433–4438. doi: 10.1016/S0032-3861(96)01039-7
[5] Sato K, Oaki Y, Imai H. Phase separation of composite materials through simultaneous polymerization and crystallization. NPG Asia Mater. 2017;9(4):e377. doi: 10.1038/am.2017.53
[6] Tishkevich DI, Grabchikov SS, Lastovskii SB, et al. Function composites materials for shielding applications: correlation between phase separation and attenuation properties. J Alloys Compd. 2019;771:238–245. doi: 10.1016/j.jallcom.2018.08.209
[7] Debnath N, Takahiko K, Harinarayan D, et al. Magnetic-field-induced phase separation via spinodal decomposition in epitaxial manganese ferrite thin films. Sci Technol Adv Mater. 2018;19(1):507–516. doi: 10.1080/14686996.2018.1482520
[8] Kim JH, Karasz FE, Malone MF. Effects of phase separation on the mechanical properties of polystyrene/poly(vinyl methyl ether) blends. Polym Eng Sci. 1991;31(13):981–987. doi: 10.1002/pen.760311308
[9] Xu C, Zheng M-X, Wei Y, et al. Liquid crystalline nanoparticles via polymerization-induced self-assembly: morphology evolution and function regulation. Chem Eur J. 2024;30(15):e202303586. doi: 10.1002/chem.202303586
[10] Matsumoto I, Sekiya R, Haino T. Self-assembly of nanographenes. Angew Chem Int Ed. 2021;60(23):12706–12711. doi: 10.1002/anie.202101992
[11] Ariga K, Michihiro N, Taizo M, et al. Self-assembly as a key player for materials nanoarchitectonics. Sci Technol Adv Mater. 2019;20(1):51–95. doi: 10.1080/14686996.2018.1553108
[12] Z-G Z, Li Y, Bisoyi HK, et al. Three-dimensional control of the helical axis of a chiral nematic liquid crystal by light. Nature. 2016;531(7594):352–356. doi: 10.1038/nature17141

[13] Sun Q-F, Iwasa J, Ogawa D, et al. Self-assembled $M_{24}L_{48}$ polyhedra and their sharp structural switch upon subtle ligand variation. Science. 2010;328 (5982):1144–1147. doi: 10.1126/science.1188605
[14] Whitesides GM, Grzybowski B. self-Assem at all scales. Sci. 2002;295(5564):2418–2421. doi: 10.1126/science.1070821
[15] Philp D, Stoddart JF. Self-assembly in natural and unnatural systems. Angew Chem Int Ed Engl. 1996;35(11):1154–1196. doi: 10.1002/anie.199611541
[16] Huc I, Lehn J-M. Virtual combinatorial libraries: dynamic generation of molecular and supramolecular diversity by self-assembly. Proc Natl Acad Sci USA. 1997;94:2106–2110. doi: 10.1073/pnas.94.6.2106
[17] Ogoshi T, Azuma S, Wada K, et al. Exciplex formation by complexation of an electron-accepting guest in an electron-donating pillar[5]arene host liquid. J Am Chem Soc. 2024;146(14):9828–9835. doi: 10.1021/jacs.3c14582
[18] Xu W, Du Y, Ma H, et al. Generation of triplet states by host-stabilized through-space conjugation for the construction of efficient supramolecular photocatalysts. Angew Chem Int Ed. 2025;64(1): e202413129. doi: 10.1002/anie.202413129
[19] Hill JP, Jin W, Kosaka A, et al. Self-assembled hexa-*peri*-hexabenzocoronene graphitic nanotube. Science. 2004;304(5676):1481–1483. doi: 10.1126/science.1097789
[20] Okumura Y, Ito K. The polyrotaxane gel: a topological gel by figure-of-eight cross-links. Adv Mater. 2001;13:485–487. doi: 10.1002/1521-4095(200104)13:7<485:AID-ADMA485>3.0.CO;2-T
[21] Olsson M, Storm R, Björn L, et al. Phase-separated polymer blends for controlled drug delivery by tuning morphology. Commun Mater. 2024;5(1):231. doi: 10.1038/s43246-024-00678-y
[22] Schmitt M, Zhang J, Lee J, et al. Polymer ligand–induced autonomous sorting and reversible phase separation in binary particle blends. Sci Adv. 2016;2 (12):e1601484. doi: 10.1126/sciadv.1601484
[23] Leibler L. Theory of microphase separation in block copolymers. Macromolecules. 1980;13(6):1602–1617. doi: 10.1021/ma60078a047
[24] Yu G, Gao J, Hummelen JC, et al. Polymer photovoltaic cells: enhanced efficiencies via a network of internal donor-acceptor heterojunctions. Science. 1995;270(5243):1789–1791. doi: 10.1126/science.270.5243.1789
[25] Schäfer C, Mony J, Olsson T, et al. Entropic mixing allows monomeric-like absorption in neat BODIPY films. Chem Eur J. 2020;26(63):14295–14299. doi: 10.1002/chem.202002463
[26] Lu F, Shinohara A, Kawamura I, et al. Room-temperature alkyl-diphenylpyrene liquefication by molecular desymmetrization. Helv Chim Acta. 2023;106 (8):e202300050. doi: 10.1002/hlca.202300050
[27] Tateyama A, Nakanishi T. Responsive molecular liquid materials. Responsive Mater. 2023;1(1): e20230001. doi: 10.1002/rpm.20230001
[28] Zheng X, Nagura K, Takaya T, et al. Quest for a rational molecular design of alkyl-distyrylbenzene liquid by substitution pattern modulation. Chem Eur J. 2023;29(21):e202203775. doi: 10.1002/chem.202203775
[29] Yamamoto Y, Lu F, Nakanishi T, et al. Liquid structures and diffusion dynamics of alkyl-pyrene liquids studied by molecular dynamics simulations. J Phys Chem B. 2023;127(21):4870–4885. doi: 10.1021/acs.jpcb.2c08385
[30] Michinobu T, Nakanishi T, Hill JP, et al. Room temperature liquid fullerenes: an uncommon morphology of C_{60} derivatives. J Am Chem Soc. 2006;128 (32):10384–10385. doi: 10.1021/ja063866z
[31] Hollamby MJ, Karny M, Bomans PHH, et al. Directed assembly of optoelectronically active alkyl–π-conjugated molecules by adding *n*-alkanes or π-conjugated species. Nat Chem. 2014;6(8):690. doi: 10.1038/nchem.1977
[32] Lu F, Takaya T, Iwata K, et al. A guide to design functional molecular liquids with tailorable properties using pyrene-fluorescence as a probe. Sci Rep. 2017;7(1):3416. doi: 10.1038/s41598-017-03584-1
[33] Narayan B, Nagura K, Takaya T, et al. The effect of regioisomerism on the photophysical properties of alkylated-naphthalene liquids. Phys Chem Chem Phys. 2018;20(5):2970–2975. doi: 10.1039/c7cp05584f
[34] Ghosh A, Yoshida M, Suemori K, et al. Soft chromophore featured liquid porphyrins and their utilization toward liquid electret applications. Nat Commun. 2019;10(1):4210. doi: 10.1038/s41467-019-12249-8
[35] Wakchaure VC, Channareddy G, Babu SS. Solvent-free organic liquids: an efficient fluid matrix for unexplored functional hybrid materials. Acc Chem Res. 2024;57(5):670–684. doi: 10.1021/acs.accounts.3c00670
[36] Isoda K, Matsubara M, Ikenaga A, et al. Reversibly/Irreversibly stimuli-responsive inks based on N-heteroacene liquids. J Mater Chem C. 2019;7 (45):14075–14079. doi: 10.1039/C9TC05195C
[37] Nakanishi T. Functional organic liquids. 1st ed. Weinheim: John Wiley & Sons; 2019.
[38] Lu F, Nakanishi T. Alkyl-π engineering in state control toward versatile optoelectronic soft materials. Sci Technol Adv Mater. 2015;16(1):014805. doi: 10.1088/1468-6996/16/1/014805
[39] Babu SS, Hollamby MJ, Aimi J, et al. Nonvolatile liquid anthracenes for facile full-colour luminescence tuning at single blue-light excitation. Nat Commun. 2013;4(1):1969. doi: 10.1038/ncomms2969
[40] Wakchaure VC, Veer SD, Nidhankar AD, et al. Polymerizable solvent-free organic liquids: a new approach for large area flexible and foldable luminescent films. Angew Chem Int Ed. 2023;62(34): e202307381. doi: 10.1002/anie.202307381
[41] Machida T, Nakanishi T. Alkyl-π functional molecular liquids towards soft electronics. J Mater Chem C. 2021;9(33):10661–10667. doi: 10.1039/D1TC00998B
[42] Zielinska A, Takai A, Sakurai H, et al. A spin-active, electrochromic, solvent-free molecular liquid based on double-decker lutetium phthalocyanine bearing long branched alkyl chains. Chem Asian J. 2018;13 (7):770–774. doi: 10.1002/asia.201800175
[43] Shinohara A, Pan C, Guo Z, et al. Viscoelastic conjugated polymer fluids. Angew Chem Int Ed. 2019;58 (28):9581–9585. doi: 10.1002/anie.201903148
[44] Sato Y, Mutoh Y, Morishita S, et al. Stimulus-responsive supercooled π-conjugated liquid and its application in rewritable media. J Phys Chem Lett. 2021;12 (11):3014–3018. doi: 10.1021/acs.jpclett.1c00247
[45] Liu H, Song W, Chen X, et al. Temperature-responsive molecular liquids based on dihydrophenazines for dynamic multicolor-fluorescent anti-counterfeiting and encryption. Mater Chem Front. 2021;5 (5):2294–2302. doi: 10.1039/D0QM00903B

[46] Omura T, Morisako S, Isoda K. Amino acid-appended pyromellitic diimide liquid materials, their photoluminescence, and the thermal response that turns the photoluminescence off. Chem Commun. 2024;60(70):9352–9355. doi: 10.1039/D4CC02229G
[47] Morikawa M-A, Yang H, Ishiba K, et al. A liquid arylazopyrazole derivative as molecular solar thermal fuel with long-term thermal stability. Chem Lett. 2020;49(6):736–740. doi: 10.1246/cl.200171
[48] Shinohara A, Yoshida M, Pan C, et al. Stretchable π-conjugated polymer electrets for mechanoelectric generators. Polym J. 2022;55(4):529–535. doi: 10.1038/s41428-022-00725-w
[49] Gupta RK, Yoshida M, Saeki A, et al. Alkyl-C_{60} liquid electrets as deformable mechanoelectric generators. Mater Horiz. 2023;10(9):3458–3466. doi: 10.1039/D3MH00485F
[50] Tateyama A, Nagura K, Yamanaka M, et al. Alkyl–π functional molecular gels: control of elastic modulus and improvement of electret performance. Angew Chem Int Ed. 2024;63(20):e202402874. doi: 10.1002/anie.202402874
[51] Isoda K, Ishiyama T, Mutoh Y, et al. Stimuli-responsive room-temperature N-heteroacene liquid: in situ observation of the self-assembling process and its multiple properties. ACS Appl Mater Interfaces. 2019;11(12):12053–12062. doi: 10.1021/acsami.8b21695
[52] Kamino BA, Bender TP, Klenkler RA. Hole mobility of a liquid organic semiconductor. J Phys Chem Lett. 2012;3(8):1002–1006. doi: 10.1021/jz300058w
[53] Kramer TJ, Babu SS, Saeki A, et al. CdSe Nanocrystal/C_{60}-liquid composite material with enhanced photoelectrochemical performance. J Mater Chem. 2012;22(42):22370–22373. doi: 10.1039/C2JM35294J
[54] Babu SS, Aimi J, Ozawa H, et al. Solvent-free luminescent organic liquids. Angew Chem Int Ed. 2012;51(14):3391–3395. doi: 10.1002/anie.201108853
[55] Nidhankar AD, Goudappagouda P, Kothavade P, et al. Thermally activated delayed fluorescent solvent-free organic liquid hybrids for tunable emission applications. Chem Asian J. 2023;18(13):e202300276. doi: 10.1002/asia.202300276
[56] Kawamura M, Kuwae H, Kamibayashi T, et al. Liquid/solution-based microfluidic quantum dots light-emitting diodes for high-colour-purity light emission. Sci Rep. 2020;10(1):14528. doi: 10.1038/s41598-020-70838-w
[57] Kobayashi N, Kasahara T, Edura T, et al. Microfluidic white organic light-emitting diode based on integrated patterns of greenish-blue and yellow solvent-free liquid emitters. Sci Rep. 2015;5(1):14822. doi: 10.1038/srep14822
[58] Sheng Z, Ding Y, Li G, et al. Solid–liquid host–guest composites: the marriage of porous solids and functional liquids. Adv Mater. 2021;33(52):2104851. doi: 10.1002/adma.202104851
[59] Lu F, Hagiwara K, Yoshizawa M, et al. Luminescence tuning with excellent colour homogeneity and steadiness using fluorescent molecular liquids. J Mater Chem C. 2019;7(9):2577–2582. doi: 10.1039/C8TC06254D
[60] Takeda T, Yamamoto S, Mitsuishi M, et al. Thermoresponsive amphipathic fluorescent organic liquid. J Phys Chem C. 2018;122(17):9593–9598. doi: 10.1021/acs.jpcc.8b01131
[61] Schäfer C, Mony J, Olsson T, et al. Effect of the aza-N-bridge and push–pull moieties: a comparative study between BODIPYs and aza-BODIPYs. J Org Chem. 2022;87(5):2569–2579. doi: 10.1021/acs.joc.1c02525
[62] Guo Z, Shinohara A, Pan C, et al. Consistent red luminescence in π-conjugated polymers with tuneable elastic moduli over five orders of magnitude. Mater Horiz. 2020;7(5):1421–1426. doi: 10.1039/D0MH00029A
[63] Lu F, Jang K, Osica I, et al. Supercooling of functional alkyl-π molecular liquids. Chem Sci. 2018;9(33):6774–6778. doi: 10.1039/C8SC02723D
[64] Tao SJ. Positronium annihilation in molecular substances. J Chem Phys. 1972;56(11):5499–5510. doi: 10.1063/1.1677067
[65] Goworek T. Positronium as a probe of small free volumes. J Nucl Radiochem Sci. 2000;1(1):11–13. doi: 10.14494/jnrs2000.1.11
[66] Zheng X, Gupta RK, Nakanishi T. Order from disorder: directed assembly of alkyl-π functional molecular liquids. Curr Opin Colloid Interface Sci. 2022;62:101641. doi: 10.1016/j.cocis.2022.101641
[67] Maeda M, Nobukawa S, Takeshita H, et al. Free volume and local dynamics in modulus-enhanced polycarbonate under addition of low-mass molecules. J Soc Mater Sci Jpn. 2023;72(1):17–22. doi: 10.2472/jsms.72.17
[68] Wang L-H, Porter RS. Miscibility of a polyarylate with a liquid crystalline copolyester. J Polym Sci Part B: Polym Phys. 1993;31(9):1067–1073. doi: 10.1002/polb.1993.090310901
[69] Brostow W, Chiu R, Kalogeras IM, et al. Prediction of glass transition temperatures: binary blends and copolymers. Mater Lett. 2008;62(17–18):3152–3155. doi: 10.1016/j.matlet.2008.02.008
[70] Van Gurp M, Palmen J. Time-temperature superposition for polymeric blends. Rheol Bull. 1998;67:5–8.
[71] Yan Z-C, Li Y, Guo Z, et al. Rheology of conjugated polymers with bulky and flexible side chains. Macromolecules. 2021;54(9):4061–4069. doi: 10.1021/acs.macromol.1c00044
[72] Shangguan Y, Chen F, Jia E, et al. New insight into time-temperature correlation for polymer relaxations ranging from secondary relaxation to terminal flow: application of a universal and developed WLF equation. Polymers. 2017;9(11):567. doi: 10.3390/polym9110567
[73] Sanditov DS, Razumovskaya IV, Mashanov AA. On the temperature dependence of the glass transition activation energy. Polym Sci Ser A. 2020;62(5):588–596. doi: 10.1134/S0965545X20050144
[74] Angell CA. Formation of glasses from liquids and biopolymers. Science. 1995;267(5206):1924–1935. doi: 10.1126/science.267.5206.1924
[75] Kube SA, Sohn S, Ojeda-Mota R, et al. Compositional dependence of the fragility in metallic glass forming liquids. Nat Commun. 2022;13(1):3708. doi: 10.1038/s41467-022-31314-3
[76] Pan C, Sugiyasu K, Takeuchi M. Blending conjugated polymers without phase separation for fluorescent colour tuning of polymeric materials through FRET. Chem Commun. 2014;50(80):11814–11817. doi: 10.1039/C4CC03594A
[77] Algar WR, Hildebrandt N, Vogel SS, et al. FRET as a biomolecular research tool–understanding its

potential while avoiding pitfalls. Nat Methods. 2019;16(9):815–829. doi: 10.1038/s41592-019-0530-8

[78] Zhu R, Luo Z, Chen H, et al. Realizing rec. 2020 color gamut with quantum dot displays. Opt Express. 2015;23(18):23680–23693. doi: 10.1364/OE.23.023680

[79] Lu F, Kitamura N, Takaya T, et al. Experimental and theoretical investigation of fluorescence solvatochromism of dialkoxyphenyl-pyrene molecules. Phys Chem Chem Phys. 2018;20(5):3258–3264. doi: 10.1039/C7CP06811E

[80] Frisch MJ, Trucks GW, Schlegel HB, et al. Gaussian 09, revision E.01. Wallingford (CT): Gaussian, Inc.; 2013.

[81] Lu T, Chen F. Multiwfn: a multifunctional wavefunction analyzer. J Comput Chem. 2012;33(5):580–592. doi: 10.1002/jcc.22885

[82] Lu T. A comprehensive electron wavefunction analysis toolbox for chemists, Multiwfn. J Chem Phys. 2024;161(8):082503. doi: 10.1063/5.0216272

[83] Humphrey W, Dalke A, Schulten K. VMD: visual molecular dynamics. J Mol Graph Model. 1996;14(1):33–38. doi: 10.1016/0263-7855(96)00018-5